# Ab initio-based prediction and TEM study of silicide precipitation in titanium

**8 authors**, including:

Daniel Poletaev
Belgorod State University
**2** PUBLICATIONS **5** CITATIONS

SEE PROFILE

D.A. Aksyonov
Skolkovo Institute of Science and Technology
**7** PUBLICATIONS **14** CITATIONS

SEE PROFILE

Sergey Sergeevich Manokhin
Belgorod State University
**15** PUBLICATIONS **20** CITATIONS

SEE PROFILE

Maxim Ivanov
Belgorod State University
**32** PUBLICATIONS **320** CITATIONS

SEE PROFILE

Some of the authors of this publication are also working on these related projects:

Project  Thermal stability mechanisms of grain boundary structure in hcp titanium View project

Project  Li-ion cathode materials View project

# Ab initio-based prediction and TEM study of silicide precipitation in titanium

D.O. Poletaev *, A.G. Lipnitskii, A.I. Kartamyshev, D.A. Aksyonov, E.S. Tkachev, S.S. Manokhin, M.B. Ivanov, Yu. R. Kolobov

The Center of Nanostructured Materials and Nanotechnologies, Belgorod State University, Belgorod, Russian Federation

## ABSTRACT

The literature contains many contradictory data about the most thermodynamically favorable structure of precipitates in $\alpha$-Ti matrix of the hypoeutectoid Ti–Si alloys. In this work we applied our recently developed thermodynamic model to predict the structure of Ti–Si precipitates in $\alpha$-Ti matrix of the Ti–Si alloy with total Si concentration of 0.7 wt.%. We considered all prominent Ti–Si phases such as $Ti_3Si$, $Ti_5Si_3$, $Ti_5Si_4$, $TiSi$ and two $TiSi_2$ phases and discovered that formation of the $Ti_5Si_3$ phase is more favorable than that of the $Ti_3Si$ in contradiction with the known phase diagrams. Theoretical result was confirmed by experimental investigation of microstructure and phase composition of the model Ti–0.7Si alloy annealed at 873 K for 10 h. Indeed, the only observed phase has hexagonal $Ti_5Si_3$ structure. To ensure the completeness of the results we calculated ab initio elastic constants for all considered Ti–Si phases.

© 2014 Elsevier B.V. All rights reserved.

## 1. Introduction

Titanium alloys containing even small amounts of Si show better corrosion resistance and mechanical properties compared with Si-free commercially pure titanium [1–6] and can be used as promising materials for medical implants [1]. Precipitation of the titanium silicides in the Ti–Si based alloys is one of the most important processes in the microstructure evolution during heat treatment. Dispersions of the silicide particles can be very effective for strengthening and improving the structural stability of such alloys [7–11]. However, there are many contradictions in the literature about the most thermodynamically favorable structure of precipitates in the $\alpha$-Ti matrix at low concentrations of Si.

According to the recently assessed Ti–Si binary phase diagram [12] the most favorable precipitating phase in $\alpha$-Ti is $Ti_3Si$ (86).[1] Indeed, the $Ti_3Si$ (86) phase was observed in the hypereutectoid Ti–Si alloys with silicon content from 1.5 to 15.3 wt.% (2.6 to 26 at.%) after long-term heat treatments at sufficiently high temperatures [13–16]; see Table 1. Existence of the $Ti_3Si$ (86) phase in the Ti–Si system was also confirmed by Kozlov and Pavlyuk [17] on the binary Ti–Si alloys annealed at 670 K for 720 h.

Nevertheless, in a number of the experimental investigations of silicide precipitation in the binary Ti–Si [18–21,1] and more complex Si-containing titanium alloys [18,22,19] the $Ti_5Si_3$ (193) phase was observed instead of $Ti_3Si$ (86).

It was found by ab initio calculations [23] that formation enthalpy of the $Ti_3Si$ (86) phase, referred to the stable structures of constituting elements, i.e. silicon with diamond structure and hcp titanium, lies above the ground-state line at 0 K. On the other hand, the $Ti_5Si_3$ (193) phase at 0 K was found to be thermodynamically stable. However, there is no diamond silicon in $\alpha$-Ti matrix and to predict thermodynamic stability of silicide precipitates another reference state for Si is needed.

Considering the underlying physical process of precipitation, the initial state of Si-low-concentration Ti–Si system is substitutional solid solution, in which Si atoms occupy lattice sites of hcp-Ti matrix. The final state is dispersed titanium silicide particles plus Si-solid solution with lower concentration. If the full energy of the system is lower in the final state, then the precipitation is thermodynamically favorable process.

The main aim of our study is to establish the most thermodynamically favorable structure of the precipitates in the $\alpha$-Ti matrix of the hypoeutectoid Ti–Si alloys at the temperatures from 0 K to the temperature of $\alpha/\beta$-Ti polymorphic transformation.

Our work consists of the theoretical and experimental parts. In the theoretical part of our study we use density functional theory

**Table 1**
Experimental conditions at which Ti₃Si (86) phase formation was observed in Ti–Si alloys.

| Alloy | Source | Temperature ($K$) | Phase composition |
|---|---|---|---|
| Ti–15.3Si[a] | Ref. [13] | 1373 (~330 h) | $Ti_3Si + \beta'$[b] |
| Ti–1.5Si | Ref. [14] | 1323 | $Ti_3Si + \beta'$ |
| Ti–1.5Si | | 1095 (257 h) | $Ti_5Si_3 + Ti_3Si + \alpha$[c] |
| Ti–1.5Si | | 1073 (~2370 h) | $Ti_3Si + \alpha$ |
| Ti–3.5Si | | 1323 | $Ti_3Si + \beta'$ |
| Ti–7.9Si | Ref. [15] | 1373 (90 h) | $Ti_5Si_3 + Ti_3Si + \beta'$ |
| Ti–7.6Si | Ref. [16] | 973 (90 h) | $Ti_3Si + \alpha$ |
| | | 1273 (6 h) | $Ti_3Si + \beta'$ |
| Ti–11.7Si | | 973 (90 h) | $Ti_3Si + \alpha$ |
| | | 1273 (6 h) | $Ti_3Si + \beta'$ |

[a] Silicon content in wt.%.
[b] $\beta'$ – solid solution of silicon in $\beta$-Ti.
[c] $\alpha$ – solid solution of silicon in $\alpha$-Ti.

(DFT) to calculate specific formation energies of Ti–Si phases in the $\alpha$-Ti matrix, accounting details of the precipitation process. It allows us to report energetically most favorable crystal structures. Using calculated energies and thermodynamic model for dilute solid solutions developed in our previous work [24], we describe distribution of Si between the matrix and Ti–Si structures up to the temperature of the polymorphic $\alpha/\beta$-Ti transformation. The model is based on the law of mass action [25], takes *ab initio* calculated formation energies of phases and as a first approximation uses only configuration entropy of the solution. To describe mechanical properties of Ti–Si particles and their influence on the Ti matrix we provide calculated elastic constants of the corresponding Ti–Si phases.

In the experimental part of our study, to confirm theoretical predictions, we examine the structure of the model Ti–0.7Si alloy. The choice of silicon concentration of 0.7 wt.% allows to avoid formation of silicides in $\beta$-Ti during process of its cooling and to produce silicide precipitation in the $\alpha$-Ti matrix only. We use transmission electron microscopy (TEM), scanning transmission electron microscopy (STEM) and high-resolution transmission electron microscopy (HRTEM) to implement microstructural, elemental and fast Fourier transform (FFT) analysis of Ti matrix and precipitates. Finally, we calculate theoretical diffraction patterns of $\alpha$-Ti matrix and the most favorable Ti–Si phase for the interpretation of experimental results.

## 2. Details of calculation

Calculations of the full energies, optimized geometries and elastic constants were performed in the framework of the density functional theory (DFT) [26,27] within the generalized gradient approximation (GGA) using the Perdew et al. [28,29] functional and projected augmented wave (PAW) method [30] (ABINIT code [31]). It was shown that GGA provides good description of basic characteristics of Ti–Si system, such as formation energies and lattice parameters of Ti–Si compounds [23]. We considered the following valence electronic states: 3s, 3p, 4s, 3d for Ti and 3s, 3p for Si. The calculations were performed using an energy cutoff of 700 eV for the plane-wave basis set and converged with respect to the k-point integration. Brillouin-zone (BZ) integrals were approximated using the special k-point sampling of Monkhorst and Pack [32]. The $12 \times 12 \times 12$ grid was used for diamond Si cell with 2 atoms and $10 \times 10 \times 6$ grid was used for hcp Ti cell with 2 atoms. For other structures k-point grid was adopted according to the size of BZ to obtain similar densities of k-points for all unit cells. The integration over the BZ was made using the Methfessel–Paxton smearing method [33] with 0.136 eV smearing width. Such choice of main parameters ensures energy convergence to 1 meV/atom. For determination of the energy of Si atom in substitutional hcp lattice site, simulation cell of 47 $\alpha$-Ti atoms with 1 Si atom was used. The size of the cell was enough to keep the specified accuracy of the total energy.

The structural relaxation was stopped when all forces acting on the atoms were converged to within 2.5 meV/Å. Method and PAW potentials were checked by computation of lattice parameters and elastic constants of $\alpha$-Ti, diamond Si and Ti₅Si₃ (193) structures; see Tables 2 and 3. The difference between our results and experiment [34,35,17,36–40] is less than 1% for lattice constants and 10% for elastic constants.

The number of independent elastic constants is determined by the crystal symmetry. There are nine, six and five independent elastic constants for orthorhombic, tetragonal and hexagonal lattices, respectively. They were deduced by applying small strains to the equilibrium lattice and determining the resulting change in the total energy. For each modulus, the total energy of the system has been calculated for nine strained lattices, obtained by multiplication of the equilibrium lattice and distortion matrices. The distortion was equal to $d = \pm 0.0025n$, where $n = 0$–4. The elastic constants were computed by fitting the energies against the distortion parameter using the second order Taylor expansion.

**Table 2**
Calculated lattice parameters compared with experimental results and results of other DFT calculations.

| Compound | Lattice parameters (Å) | | |
|---|---|---|---|
| | GGA (our) | GGA (other) | Exp. (other) |
| $\alpha$-Ti | $a = 2.937$, $c = 4.649$ | – | $a = 2.951$, $c = 4.686$[a] |
| Diamond-Si | $a = 5.438$ | – | $a = 5.430$[b] |
| Ti₃Si (86) | $a = 10.144$, $c = 5.064$ | $a = 10.141$, $c = 5.059$[c] | $a = 10.159$, $c = 5.085$[d] |
| Ti₅Si₃ (193) | $a = 7.454$, $c = 5.119$ | $a = 7.463$, $c = 5.132$[c] | $a = 7.445$, $c = 5.143$[d] |
| | | | $a = 7.460$, $c = 5.152$[e] |
| Ti₅Si₄ (92) | $a = 6.691$, $c = 12.165$ | $a = 6.710$, $c = 12.181$[c] | $a = 7.133$, $c = 12.977$[d] |
| TiSi (62) | $a = 6.517$, $b = 3.634$, $c = 4.993$ | $a = 6.537$, $b = 3.643$, $c = 5.000$[c] | $a = 6.609$, $b = 3.593$, $c = 5.006$[d] |
| TiSi₂ (70) | $a = 8.222$, $b = 4.780$, $c = 8.533$ | $a = 8.268$, $b = 4.806$, $c = 8.560$[c] | $a = 8.258$, $b = 4.796$, $c = 8.543$[d] |
| TiSi₂ (63) | $a = 3.532$, $b = 13.490$, $c = 3.565$ | $a = 3.541$, $b = 13.617$, $c = 3.576$[c] | $a = 3.550$, $b = 13.490$, $c = 3.550$[g] |
| | | $a = 3.507$, $b = 13.440$, $c = 3.531$[f] | |

[a] Ref. [34] – lattice parameters are measured at 301 K.
[b] Ref. [35] – lattice parameters are measured at 298 K.
[c] Ref. [23].
[d] Ref. [17] – lattice parameters are measured at 670 K.
[e] Ref. [36].
[f] Ref. [44].
[g] Ref. [37].

**Table 3**
Elastic constants ($C_{ij}$ in GPa) for Ti, Si and Ti5Si3 (193). The experimental values for α-Ti are measured at 4 K [38], for diamond Si at 4.2 K [39] and for Ti5Si3 (193) [40] at room temperature.

| | $C_{11}$ | $C_{12}$ | $C_{44}$ | $C_{13}$ | $C_{33}$ | $C_{66}$ | $B$ |
|---|---|---|---|---|---|---|---|
| *α-Ti* | | | | | | | |
| GGA (our) | 176 | 84 | 45 | 75 | 191 | – | – |
| GGA[a] | 176 | 86 | 45 | 76 | 191 | – | – |
| GGA[b] | 172 | 82 | 45 | 75 | 190 | – | – |
| Exp.[c] (4 K) | 176 | 87 | 51 | 68 | 191 | – | – |
| *Diamond-Si* | | | | | | | |
| GGA (our) | 158 | 59 | 76 | – | – | – | 92 |
| Exp.[d] (4.2 K) | 167 | 65 | 80 | – | – | – | 98 |
| *Ti5Si3 (193)* | | | | | | | |
| GGA (our) | 286 | 112 | 95 | 52 | 272 | 87 | 142 |
| GGA[e] | 282 | 116 | 92 | 59 | 261 | 83 | 143 |
| GGA[f] | 289 | 106 | 97 | 56 | 274 | 92 | 143 |
| Exp.[g] (298 K) | 285 | 106 | 93 | 53 | 268 | 89 | 140 |

[a] Ref. [24].
[b] Ref. [45].
[c] Ref. [38].
[d] Ref. [39].
[e] Ref. [46].
[f] Ref. [47].
[g] Ref. [40].

The distortion matrices for tetragonal and orthorhombic crystals were taken from Refs. [41,42] and for hexagonal crystals from Ref. [43]. Relaxation of the internal degrees of freedom was carried out for all applied deformations.

To ensure that used PAW potentials correctly reproduce the energy characteristics of the Ti–Si system, we calculated formation enthalpies of titanium silicides from Ti (hcp) and Si (diamond) at 0 K and compared them with experimental and other theoretical results; see Table 4. To calculate the formation enthalpies we used the following equation:

$$\Delta_f H = \frac{E(Ti_x Si_y) - xE(Ti_{hcp}) - yE(Si_{dia})}{x + y}, \tag{1}$$

where $E(Ti_x Si_y)$ is the total energy of simulation cell with $x + y$ atoms, $E(Ti_{hcp})$ is the energy of one Ti atom in bulk α-Ti, $E(Si_{dia})$ is the energy of one Si atom in diamond structure.

The difference in formation enthalpies between our results and optimized CALPHAD results [12] is less than 5%. Other experimental values of the formation enthalpies for Ti5Si3 (193), Ti5Si4 (92), TiSi (62) and TiSi2 (70) compounds have been obtained by mass spectrometry [48] and by direct reaction calorimetry [49]. For the TiSi2 (70) compound another experimental value of the formation enthalpy was obtained by Topor and Kleppa [50], who had used solute–solvent drop calorimetry. The difference between these experimental formation enthalpies and our calculated formation enthalpies is less than 7%.

## 3. Details of experiment

The model Ti–0.7Si alloy was prepared using vacuum levitation melting from high purity (99,997%) powders of Ti and Si in appropriate proportions. Obtained material was annealed in laboratory furnace Nabertherm at 873 K for 10 h. The alloy samples were mechanically polished after annealing using sandpaper of the different grits. The final polishing was performed using colloidal silica suspension ($SiO_2$ with crystallite size of the order of 0.04 μm). Thin foils for transmission electron microscopy were prepared by mechanical grinding-polishing using a Struers plant LaboPol-5 and the subsequent jet polishing on a plant TenuPol-5 using electrolyte $20\%HClO_4 + 80\%CH_3CO_2H$.

To examine the structure of annealed metal a transmission electron microscope Tecnai G2 F20 S-TWIN was used. An accelerating voltage of 200 keV in transmission electron microscopy (TEM) mode and in scanning transmission electron microscopy (STEM) mode was used. The distribution of chemical elements was determined by energy dispersive X-ray analysis (EDX) in STEM mode using the EDAX console, TIA, and Genesis Microanalysis software. To determine lattice geometry of the matrix and precipitated dispersed particles, fast Fourier transform (FFT) analysis of high-resolution TEM images was performed.

## 4. Results and discussion

### 4.1. Formation energies of Ti–Si phases in α-Ti at 0 K

The formation energies of phases in the metallic matrix depend on the underlying physics. In our case dispersed particles are formed from substitutional Si solid solution at low Si concentrations. To justify our choice of substitutional solid solution, we compare calculated energies of one Si atom in the substitutional position $E(Si_{sol})$ and one Si atom in octahedral interstitial position $E(Si_{oct})$ in the α-Ti lattice. $E(Si_{oct})$ is the difference between the total energy of 48 Ti atoms supercell with 1 Si atom in octahedral interstitial position and energy of the same supercell without Si; $E(Si_{sol})$ is the analogous difference but for Si substitutional position. It was found that $E(Si_{sol})$ is lower than $E(Si_{oct})$ by 2.166 eV.

Hence: (i) we use the energy of Si atom in substitutional position in α-Ti as the energy reference; (ii) to compare energetic favorability of Ti–Si phases in α-Ti we use specific formation energy $\Delta E$ normalized to the number of Si atoms in the phase; (iii) we consider each Ti–Si phase as a set of non-interacting associates containing one Si atom and neglect the interface energy between Ti matrix and the Ti–Si phase. Such consideration allows to use our thermodynamic model [24], which will be briefly described in Section 4.2.

The specific formation energy of an arbitrary Ti–Si phase in α-Ti was calculated as follows:

$$\Delta E = \frac{E(Ti_x Si_y) - xE(Ti_{hcp}) - yE(Si_{sol})}{y}, \tag{2}$$

**Table 4**
Calculated formation enthalpies ($\Delta_f H$) of Ti–Si phases referred to Ti (hcp) and Si (diamond) compared with experimental results and results of other DFT calculations.

| Compound | $\Delta_f H$ (kJ/mol) | | | | |
|---|---|---|---|---|---|
| | GGA (our) | GGA [23] | CALPHAD [12] | Exp. [48] | Exp. [49,50] |
| Ti3Si (86) | −48.84 | −47.11 | −50.00 | – | – |
| Ti5Si3 (193) | −74.99 | −72.53 | −72.95 | −78.10 ± 5 | −73.80 ± 2 |
| Ti5Si4 (92) | −77.24 | −74.63 | −79.00 | −75.90 ± 5 | −78.50 ± 2.1 |
| TiSi (62) | −75.94 | −72.23 | −77.53 | −71.50 ± 5 | −72.60 ± 1.9 |
| TiSi2 (70) | −54.95 | −49.87 | −58.35 | −53.50 ± 5 | −57.00 |
| TiSi2 (63) | −55.78 | −51.3 | −57.00 | – | – |

where $E(Ti_xSi_y)$ is the total energy of simulation cell with $x + y$ atoms, $E(Ti_{hcp})$ is the energy of one Ti atom in bulk $\alpha$-Ti, $E(Si_{sol})$ is the energy of Si atom in substitutional position in $\alpha$-Ti as defined above. The specific formation energy of the Ti–Si phase is equal to the formation energy of the Ti-Si associate containing one Si atom. Introducing the specific formation energy we consider the process of the Ti-Si phase formation as a transition of Si atom from the dilute solid solution of substitutional Si atoms to the dilute solid solution of Ti-Si associates. The associates, in turn, are forming $Ti_xSi_y$ particles in $\alpha$-Ti matrix.

We have calculated $\Delta E$ for six fully relaxed Ti–Si phases known from the recently assessed binary Ti–Si phase diagram [12]. Detailed description of the orthorhombic $TiSi_2$ (70) and $TiSi_2$ (63) structures can be found in Ref. [51], orthorhombic TiSi (62), tetragonal $Ti_3Si$ (86), $Ti_5Si_4$ (92) and hexagonal $Ti_5Si_3$ (193) in Ref. [23]. Specific formation energies $\Delta E$ in comparison with the calculated formation enthalpies $\Delta_f H$ of these phases are summarized in Table 5.

According to Table 5, if we consider formation of the Ti–Si phase with the reference state of Si in diamond structure, the most energetically favorable phases are $Ti_5Si_4$ (92), TiSi (62) and $Ti_5Si_3$ (193). On the contrary, if we choose the Si substitutional solid solution as a reference state, the most energetically favorable phases are $Ti_5Si_3$ (193) and $Ti_3Si$ (86). The $Ti_5Si_3$ (193) phase has the most negative specific formation energy, which is lower by 48 meV/atom-Si in comparison to specific formation energy of the $Ti_3Si$ (86) phase. Therefore, the $Ti_5Si_3$ (193) phase should precipitate in the first place.

According to the literature data on the Ti–Si system, the $Ti_3Si$ (86) phase is formed by peritectoid reaction between $\beta$-Ti or $\alpha$-Ti and the $Ti_5Si_3$ (193) phase. The reaction was observed in experimental investigations in the range of temperatures from 670 K [17] to 1323 K [14]. However, it is not clear if the peritectoid reaction is energetically favorable at lower temperatures.

Fortunately, this can be easily checked by the calculation from first-principles. The change of energy in the reaction (at 0 K)

$$4Ti(hcp) + Ti_5Si_3 \rightarrow 3Ti_3Si$$
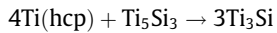
is $3E[Ti_3Si] - 4E[Ti(hcp)] - E[Ti_5Si_3] = 0.143$ eV. It means that the flow of such reaction is energetically unfavorable at 0 K.

In conclusion to this section it should be noted that the results obtained for zero temperature could be not appropriate for higher temperatures. An extrapolation of the results to the finite-temperature region requires the usage of a suitable thermodynamic model, one of which will be described in the following section.

### 4.2. Equilibrium between Ti–Si precipitates and solid solution of silicon in $\alpha$-titanium

All silicon at 0 K must occupy the lowest energy state, which is $Ti_5Si_3$ (193) phase according to our data. However, in the case of industrial heat treatments it is important to know the influence of temperature on the phase formation. To predict possible structure of precipitates at finite temperatures, we use special model which is based on the approach of chemical reactions rates and

concept of associated solutions [52–54]. The details of the model can be found in our previous work dealing with Ti–C system [24]. In the present paper we briefly repeat the main equations of the model for the case of the Ti–Si system.

Equilibrium between each $Ti_xSi_y$ particle and solid solution of Si in $\alpha$-Ti can be described within the quasi-chemical reaction:

$$Ti_m(hcp) + Si(sol) \rightarrow Ti_mSi(j), \tag{3}$$

where $Ti_mSi(j)$ is an associate of one Si atom and $m = x/y$ Ti atoms having $j$ structure. Eq. (3) describes the transition of one Si atom from the solid solution into the $Ti_xSi_y$ structure which is considered as a set of non-interacting associates $Ti_mSi(j)$. The $Ti_mSi(j)$ associates in the $Ti_xSi_y$ structure do not interact with each other because the energy related to the one associate is independent of the size and shape of the $Ti_xSi_y$ particle. In the limit of the large enough particles [18,20] we neglect the interface energy between Ti matrix and precipitates with $Ti_xSi_y$ structure.

At low Si concentrations we can use approximation of dilute solid solution, which states that the average distances between solute atoms are much larger than their radii of interaction, and one can neglect the interaction between different Si atoms in the Ti matrix. In this case the law of mass action [25] for Eq. (3) can be written as follows:

$$K(j) = \frac{m(j)[Ti_mSi(j)]}{[Ti(hcp)][Si(sol)]}, \tag{4}$$

where $K(j)$ is the generation rate constant of $Ti_mSi(j)$ associate, $[Ti_mSi(j)]$, $[Ti(hcp)]$ and $[Si(sol)]$ are the concentrations of the $Ti_mSi(j)$ associates in Ti matrix, Ti atoms in hcp lattice and Si atoms in substitutional positions of hcp-Ti lattice, respectively. On the other hand, the generation rate constant $K(j)$ is defined by equation:

$$K(j) = A(j, T)e^{-\Delta G\beta}, \tag{5}$$

where $\beta = 1/k_B T$, $\Delta G = \Delta E - T\Delta S$ is change of Gibbs free energy at zero pressure and $A(j, T)$ is pre-exponential factor. We take $A(j, T) = 1$ for all structures and temperatures because we consider a dilute solid solution. The $\Delta E$ is the specific formation energy of $Ti_mSi(j)$ associate as it is defined in Section 4.1. The change of entropy $\Delta S$ was calculated as

$$\Delta S = -k_B \left( 1 + \frac{[Si(sol)]}{[Ti(hcp)]} - \ln \frac{[Si(sol)]}{[Ti(hcp)]} \right). \tag{6}$$

We consider only configuration entropy of Si solid solution, because it is the main contribution in the full entropy. We neglect the vibrational entropy of the Ti–Si phases and the configurational entropy of ideal solutions of the $Ti_mSi(j)$ associates because their positions are restricted by $j$ structures.

To find the temperature dependence of Si atoms contributions to the Ti–Si structures, we solve self-consistently the following system of equations:

$$\begin{cases} [Si(sol)] + \sum_j [Ti_mSi(j)] = x_{Si} \\ [Ti(hcp)] + \sum_j m(j)[Ti_mSi(j)] = x_{Ti} , \\ d_{Si}(j) = \frac{K(j)}{m(j)x_{Si}}[Ti(hcp)][Si(sol)] \end{cases} \tag{7}$$

where $x_{Si}$ and $x_{Ti}$ are the total concentrations of Si and Ti atoms in the system, respectively. Fractions of all silicon atoms in precipitates with $j$ structure $d_{Si}(j) = [Ti_mSi(j)]/x_{Si}$ are the main obtained values. To solve the system and calculate $d_{Si}(j)$ we additionally use the value of $[Ti_mSi(j)]$ derived from the Eq. (4).

The values of $d_{Si}(j)$ depend on the specific formation energies $\Delta E$ and can be interpreted as formation probabilities of the precipitates with $j$ structure. We calculated values of $d_{Si}(j)$ only for phases with negative specific formation energies. The temperature

**Table 5**
Specific formation energies $\Delta E$ (Eq. (2)) in comparison with formation enthalpies $\Delta_f H$ (Eq. (1)) of Ti–Si phases at 0 K.

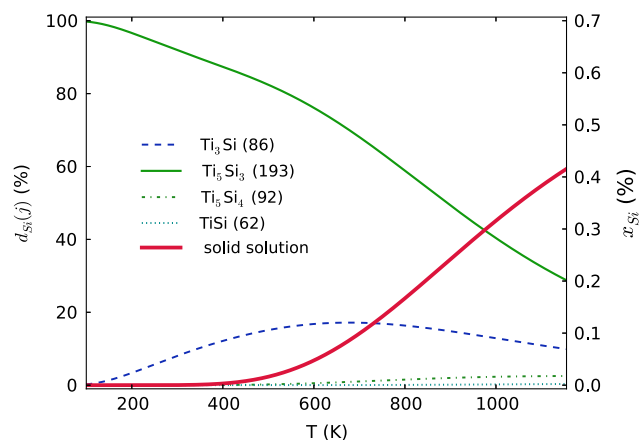| Phase | $\Delta E$ (meV/atom-Si) | $\Delta_f H$ (meV/atom) |
|---|---|---|
| $Ti_3Si$ (86) | −526 | −506 |
| $Ti_5Si_3$ (193) | −574 | −777 |
| $Ti_5Si_4$ (92) | −303 | −801 |
| TiSi (62) | −76 | −787 |
| $TiSi_2$ (70) | 644 | −569 |
| $TiSi_2$ (63) | 631 | −578 |

**Fig. 1.** Temperature dependence of silicon atoms contributions $d_{Si}(j)$ to the Ti–Si structures and Si solid solution. Total silicon concentration $x_{Si}$ is 0.7 wt.%.
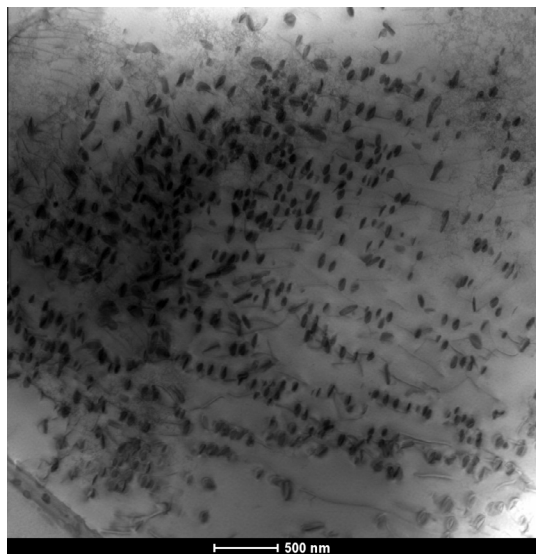


**Fig. 2.** Distribution of the titanium silicide particles in the $\alpha$-Ti matrix. TEM image.

dependence of $d_{Si}(j)$ up to the temperature of polymorphic $\alpha$-Ti/$\beta$-Ti transformation (1156 K) is shown in Fig. 1. We have used total Si concentration of 0.7 wt.% in order to compare our theoretical predictions and experimental results obtained for the Ti–0.7Si alloy.

There are five phases in the thermodynamic equilibrium in accordance with the number of constituents in the Ti–Si system: the Si solid solution and four types of associates $Ti_mSi(j)$. The Si atoms are mainly distributed by the $Ti_5Si_3$ (193) and $Ti_3Si$ (86) phases in the 200–1156 K region. It means that there is a probability of precipitation of mostly two phases in this temperature interval. The $Ti_5Si_3$ (193) phase has the highest probability of precipitation, whereas precipitation of the $Ti_3Si$ (86) phase from the Si solid solution is quite small.

With the rise of temperature, the contribution of Si in the solid solution increases due to the configuration entropy. According to our model, the concentration of Si in solid solution at the temperature of polymorphic $\alpha/\beta$-Ti transformation shows the solubility limit of Si in $\alpha$-Ti at the given total concentration of Si. The calculated solubility limit of $\sim$0.41 wt.% at 1156 K lies in the range of the experimental solubility limits between 0.30 wt.% at 1138 K [55] and 0.47 wt.% at 1133 K [56].

### 4.3. Experimental results

Our theoretical calculations allowed us to establish the most energetically favorable structure of precipitates in the $\alpha$-Ti matrix in the temperature range of 0–1156 K and Si concentration of 0.7 wt.%. However, to show that made assumptions, such as the neglect of vibrational entropy and the omission of the interface energy between Ti matrix and Ti–Si compounds, are reasonable, we provide experimental confirmation of the theoretical predictions. Below we describe results of experimental structure investigation of the Ti–0.7Si alloy prepared by the vacuum levitation melting and heat treatment at 873 K for 10 h.

We detected dispersed titanium silicide particles with the average size of 250 nm in the $\alpha$-Ti matrix of the heat treated Ti–0.7Si alloy by the TEM and STEM methods; see Figs. 2 and 3.

Dispersed particles are distributed essentially by grains of the $\alpha$-Ti matrix. The energy dispersive X-ray analysis (EDX) showed that the concentration of Si in particles significantly exceeds that in the Ti matrix and varies from 20 to 40 at.%; see Fig. 4.

To define the crystal structure of the very small precipitates we were forced to use high-resolution transmission electron microscopy (HRTEM) technique. The images obtained in HRTEM mode and their Fourier patterns (Figs. 5 and 6) show that dispersed silicide particles have hexagonal structure with lattice parameters
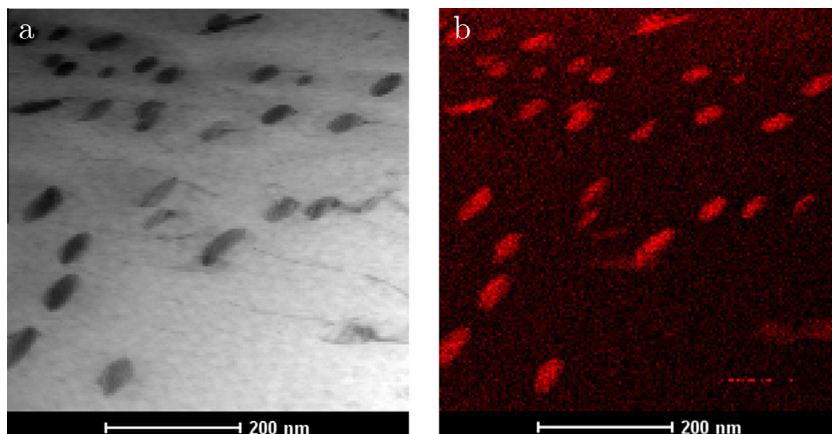


**Fig. 3.** (a) STEM image showing distribution of titanium silicide particles in $\alpha$-Ti matrix in the heat treated Ti–0.7Si alloy. (b) Element mapping showing distribution of silicon atoms by matrix and particles.

**Fig. 5.** (a) HRTEM image of titanium silicide (2) in α-Ti matrix (1) and (b) Fourier pattern from whole area. Zone axis of α-Ti matrix is [2̄1̄10]. Zone axis of titanium silicide particle is [21̄10].



**Fig. 6.** (a) Fourier pattern from Ti matrix. (b) Fourier pattern from silicide. (c) Calculated diffraction pattern of the hcp-Ti. (d) Calculated diffraction pattern of the Ti₅Si₃ (193). Zone axis is [21̄10].

**Fig. 4.** Results of energy dispersive X-ray analysis of dispersed particles (1) and titanium matrix (2).

close to the stoichiometric titanium silicide Ti₅Si₃ (193). The orientation relationships between particles and matrix are $(0001)_{Ti}\|(0001)_{silicide}$ and $[2\bar{1}\bar{1}0]_{Ti}\|[2\bar{1}\bar{1}0]_{silicide}$. The $(0001)_{Ti}\|(0001)_{silicide}$ orientation relationship between α-Ti matrix and $(Ti,Zr)_5Si_3$ precipitates was found previously by Flower et al. [18] in ternary Ti–1Si–5Zr alloys after aging at 823 K.

To compare the theoretical and the experimental results we calculated theoretical diffraction patterns of hcp-Ti and Ti₅Si₃ (193) compound. We included forbidden reflexes on the calculated

**Table 6**
Interplanar spacings in α-titanium matrix and titanium silicide calculated from Fourier patterns and compared with tabulated and first-principles data.

| Phase | (002) | (010) | (011) |
|---|---|---|---|
| α-Ti_ss | | | |
| $d_{exp}$, Å | 2.423 | 2.604 | 2.284 |
| $d_{calc}$, Å | 2.325 | 2.544 | 2.232 |
| $d_{tab}$, Å | 2.341 | 2.558 | 2.244 |
| Ti₅Si₃ | | | |
| $d_{exp}$, Å | 2.644 | 2.480 | 2.230 |
| $d_{calc}$, Å | 2.559 | 2.152 | 1.984 |

**Table 7**
Theoretical values of the elastic constants $C_{ij}$ (in GPa) of Ti–Si phases.

| Phase | $C_{11}$ | $C_{12}$ | $C_{44}$ | $C_{33}$ | $C_{13}$ | $C_{22}$ | $C_{23}$ | $C_{55}$ | $C_{66}$ | $B$ |
|---|---|---|---|---|---|---|---|---|---|---|
| Ti$_3$Si (86) | 246 | 86 | 83 | 257 | 69 | – | – | – | 102 | 133 |
| Ti$_5$Si$_3$ (193) | 286 | 112 | 95 | 272 | 52 | – | – | – | 87 | 142 |
| Ti$_5$Si$_4$ (92) | 289 | 77 | 106 | 311 | 66 | – | – | – | 128 | 145 |
| TiSi$_2$ (63) | 278 | 49 | 131 | 317 | 96 | 242 | 70 | 139 | 118 | 141 |
| TiSi$_2$ (70) | 412 | 62 | 126 | 319 | 43 | 324 | 26 | 95 | 151 | 147 |
| TiSi (62) | 241 | 113 | 102 | 344 | 58 | 286 | 62 | 114 | 151 | 149 |

diffraction patterns to compare them conveniently with the Fourier patterns of HRTEM images (Fig. 6) for which the forbidden reflexes appear during the image construction.

Interplanar spacings in α-Ti $d_{exp}$(Ti) and Ti$_5$Si$_3$ $d_{exp}$(Ti$_5$Si$_3$) were calculated from the Fourier patterns (Fig. 6) and compared with those obtained from first-principles results, $d_{calc}$(Ti) and $d_{calc}$(Ti$_5$Si$_3$), and well-known tabulated data; see Table 6. Although the $d_{exp}$(Ti) and $d_{exp}$(Ti$_5$Si$_3$) are larger than $d_{calc}$(Ti) and $d_{calc}$(Ti$_5$Si$_3$), the positions of reflexes on the Fourier patterns are similar to the positions of reflexes on the theoretical diffraction patterns. This confirms that titanium silicide particles have hexagonal lattice. There is only one hexagonal phase in the Ti–Si system and it is Ti$_5$Si$_3$ (193).

Hence, comparison of calculated diffraction patterns and Fourier patterns of experimental HRTEM images confirms our theoretical predictions, according to which the hexagonal Ti$_5$Si$_3$ (193) phase should mainly precipitate in α-Ti from the dilute Si solid solution.

### 4.4. Elastic constants of Ti–Si phases

To make qualitative estimation of the Ti–Si particles influence on the strength characteristics of titanium alloys, we calculated elastic constants of corresponding Ti–Si phases. The elastic constants provide information about the bonding characteristics between adjacent atomic planes, anisotropic character of the bonding, and structural stability. Elastic constants have correlations with ideal shear strengths [57]. Table 7 shows calculated elastic constants of all Ti–Si phases known from the phase diagram [12].

Elastic constants of all Ti–Si phases are higher than that of pure α-Ti. Hence, the microstructural design of Ti–Si alloys based on the precipitation of titanium silicides seems to be one of the most effective way of obtaining Ti–Si alloys with high mechanical characteristics.

## 5. Conclusions

In our work we used PAW GGA plane-wave method to calculate specific formation energies of Ti–Si phases in α-Ti. We found that at low concentrations of Si the most thermodynamically favorable phase at 0 K is Ti$_5$Si$_3$ (193). This is in contrast to Ti$_3$Si (86) phase, which is expected from the Ti–Si binary phase diagram [12]. According to our calculations, the formation of the Ti$_3$Si (86) phase from α-Ti and Ti$_5$Si$_3$ (193) phases is energetically unfavorable at 0 K.

Further, we predicted probabilities of the Ti–Si phases formation in the dependence of temperature using our developed model [24], which is based on the specific formation energies and the law of mass action. According to the model, considering only configuration entropy of Si solid solution, the concurrent existence of Ti$_5$Si$_3$ (193) and Ti$_3$Si (86) phases is possible in α-Ti at the temperatures from 200 K to the temperature of polymorphic α/β-Ti transformation. The Ti$_5$Si$_3$ (193) is the most favorable phase in this temperature interval.

To confirm our theoretical predictions we carried out the experimental investigation of the Ti–0.7Si alloy structure. Our theoretical prediction of the most favorable silicide phase in α-Ti is consistent with the experimental investigation. Indeed, we observed formation of dispersed titanium silicide particles with hexagonal structure and lattice parameters close to the Ti$_5$Si$_3$ (193) compound.

The calculated elastic constants of all Ti–Si phases including the most favorable Ti$_5$Si$_3$ (193) phase are higher than the elastic constants of pure α-Ti.

Finally, we showed that previously proposed [24] theoretical approach is suitable for the prediction of precipitates structure for the case of dilute Si solid solution in α-Ti.

## References

[1] H.-C. Hsu, S.-C. Wu, S.-K. Hsu, Y.-C. Li, W.-F. Ho, Intermetallics 47 (2014) 11–16.
[2] C.J. Rosa, Oxidat. Metals 17 (1982) 359–369.
[3] A.M. Chaze, C. Coddet, Oxidat. Metals 27 (1987) 1–20.
[4] D. Vojtech, B. Bartova, T. Kubatik, Mater. Sci. Eng.: A 361 (2003) 50–57.
[5] D. Vojtech, H. Cizova, K. Jurek, J. Maixner, J. Alloys Compd. 394 (2005) 240–249.
[6] Z. Jiang, X. Dai, H. Middleton, Mater. Sci. Eng.: B 176 (2011) 79–86.
[7] J. Zhu, A. Kamiya, T. Yamada, A. Watazu, W. Shi, K. Naganuma, Mater. Trans. 42 (2001) 336–341.
[8] J.-M. Oh, J.-W. Lim, B.-G. Lee, C.-Y. Suh, S.-W. Cho, S.-W. Lee, G.-S. Choi, Mater. Trans. 51 (2010) 2009–2012.
[9] D. Handtrack, F. Despang, C. Sauer, B. Kieback, N. Reinfried, Y. Grin, Mater. Sci. Eng.: A 437 (2006) 423–429.
[10] D. Handtrack, C. Sauer, B. Kieback, J. Mater. Sci. 43 (2007) 671–679.
[11] L. Huang, S. Wang, L. Geng, B. Kaveendran, H. Peng, Compos. Sci. Technol. 82 (2013) 23–28.
[12] H. Seifert, H. Lukas, G. Petzow, Z. Metall. 87 (1996) 2–13.
[13] W. Wakelkamp, F. van Loo, R. Metselaar, J. Eur. Ceram. Soc. 8 (1991) 135–139.
[14] N.H. Salpadoru, H.M. Flower, Metall. Mater. Trans. A 26 (1995) 243–257.
[15] A.S. Ramos, C.A. Nunes, G.C. Coelho, Mater. Character. 56 (2006) 107–111.
[16] A.M. Silva Costa, G.F. Lima, G. Rodrigues, C.A. Nunes, G.C. Coelho, P.A. Suzuki, J. Phase Equilib. Diffus. 31 (2009) 22–27.
[17] A. Kozlov, V. Pavlyuk, J. Alloys Compd. 367 (2004) 76–79.
[18] H.M. Flower, P.R. Swann, D.R.F. West, Metall. Mater. Trans. B 2 (1971) 3289–3297.
[19] M. Winstone, R.D. Rawlings, D. West, J. Less Common Metals 39 (1975) 205–217.
[20] L. Chumbley, B. Muddle, H. Fraser, Acta Metall. 36 (1988) 299–310.
[21] Y. Zhan, X. Zhang, J. Hu, Q. Guo, Y. Du, J. Alloys Compd. 479 (2009) 246–251.
[22] R.G. Nichols, H.M. Flower, D.R.F. West, J. Mater. Sci. 8 (1973) 261–264.
[23] C. Colinet, J.-C. Tedenac, Intermetallics 18 (2010) 1444–1454.
[24] D. Aksyonov, A. Lipnitskii, Y. Kolobov, Comput. Mater. Sci. 65 (2012) 434–441.
[25] A. Koudriavtsev, R.F. Jameson, W. Linert, The Law of Mass Action, Springer, Berlin Heidelberg, 2001.
[26] P. Hohenberg, Phys. Rev. 136 (1964) B864–B871.
[27] W. Kohn, L.J. Sham, Phys. Rev. 140 (1965) A1133–A1138.
[28] J. Perdew, K. Burke, Y. Wang, Phys. Rev. B 54 (1996) 16533–16539.
[29] J.P. Perdew, K. Burke, M. Ernzerhof, Phys. Rev. Lett. 77 (1996) 3865–3868.
[30] P.E. Blochl, Phys. Rev. B 50 (1994) 17953–17979.
[31] X. Gonze, J.-M. Beuken, R. Caracas, F. Detraux, M. Fuchs, G.-M. Rignanese, L. Sindic, M. Verstraete, G. Zerah, F. Jollet, M. Torrent, A. Roy, M. Mikami, P. Ghosez, J.-Y. Raty, D. Allan, Comput. Mater. Sci. 25 (2002) 478–492.
[32] H.J. Monkhorst, J.D. Pack, Phys. Rev. B 13 (1976) 5188–5192.
[33] M. Methfessel, A. Paxton, Phys. Rev. B 40 (1989) 3616–3621.
[34] R.R. Pawar, V.T. Deshpande, Acta Crystallograph. Sect. A 24 (1968) 316–317.
[35] R.O.A. Hall, Acta Crystallograph. 14 (1961) 1004–1005.
[36] J. Williams, Structure and High-temperature Properties of Ti$_5$Si$_3$ with Interstitial Additions, Ph.D. Thesis, Iowa State University, 1999.
[37] J.F. Jongste, O.B. Loopstra, G.C.a.M. Janssen, S. Radelaar, J. Appl. Phys. 73 (1993) 2816.
[38] E. Fisher, C. Renken, Phys. Rev. 135 (1964) A482–A494.
[39] J. Hall, Phys. Rev. 161 (1967) 756–761.

[40] K. Kishida, M. Fujiwara, H. Adachi, K. Tanaka, H. Inui, Acta Mater. 58 (2010) 846–857.
[41] X. Meng, X. Wen, G. Qin, Comput. Mater. Sci. 49 (2010) S372–S377.
[42] M.K. Niranjan, Intermetallics 26 (2012) 150–156.
[43] L. Fast, J. Wills, B. Johansson, O. Eriksson, Phys. Rev. B 51 (1995) 17431–17438.
[44] G. Shao, Acta Mater. 53 (2005) 3729–3736.
[45] R. Hennig, T. Lenosky, D. Trinkle, S. Rudin, J. Wilkins, Phys. Rev. B 78 (2008) 054121.
[46] X.-J. Chen, Z.-S. Mo, R.-N. Wang, M.-X. Zeng, B.-Y. Tang, L.-M. Peng, W.-J. Ding, J. Solid State Chem. 194 (2012) 127–134.
[47] H.-y. Wang, W.-p. Si, S.-l. Li, N. Zhang, Q.-c. Jiang, J. Mater. Res. 25 (2011) 2317–2324.

[48] R.J. Kematick, C.E. Myers, Chem. Mater. 8 (1996) 287–291.
[49] S. Meschel, O. Kleppa, J. Alloys Compd. 267 (1998) 128–135.
[50] L. Topor, O.J. Kleppa, Metall. Trans. A 17 (1986) 1217–1221.
[51] T. Wang, J.-A. Chen, X. Ling, Y.-B. Dai, Q.-Y. Dai, Modern Phys. Lett. B 20 (2006) 343–351.
[52] F. Sommer, Z. Metall. 73 (1982) 72–76.
[53] R. Schmid, Y. Chang, Calphad 9 (1985) 363–382.
[54] F. Sommer, J. Non-Crystall. Solids 117–118 (1990) 505–512.
[55] J. Murray, Binary Phase Diagrams of Ti Alloys, ASM, 1987.
[56] P.C.C. Vahlas, E. Blanquet, CALPHAD 13 (1989) 273–292.
[57] W. Luo, D. Roundy, M. Cohen, J. Morris, Phys. Rev. B 66 (2002) 1–7.